SUPPLEMENTAL INFORMATION

SUPPLEMENTAL FIGURES

Figure S1

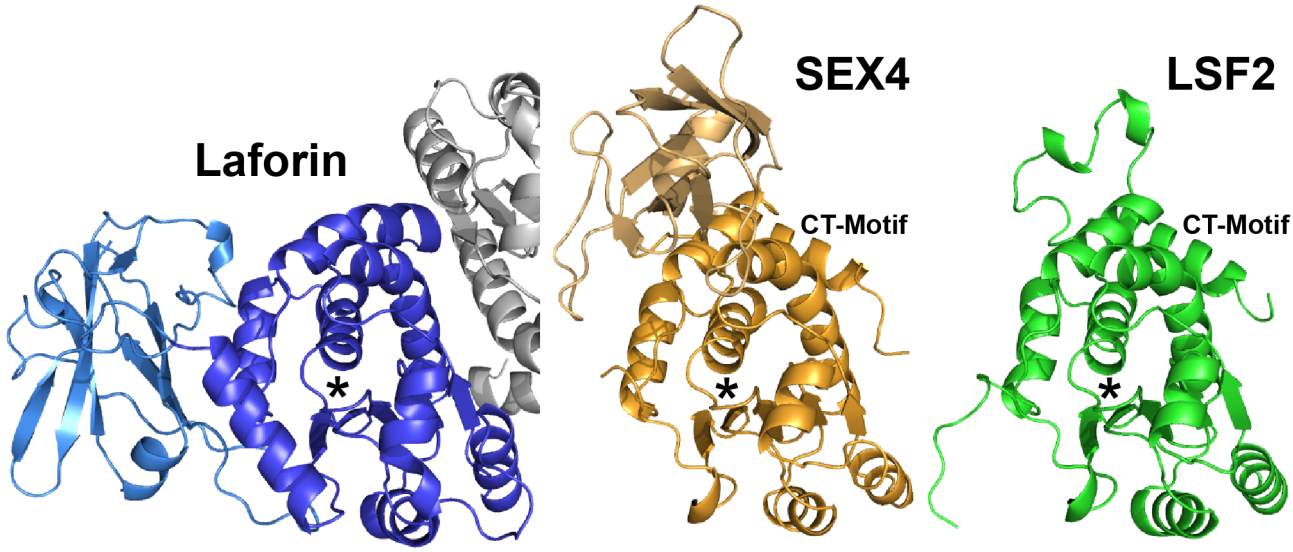

Figure S2

A

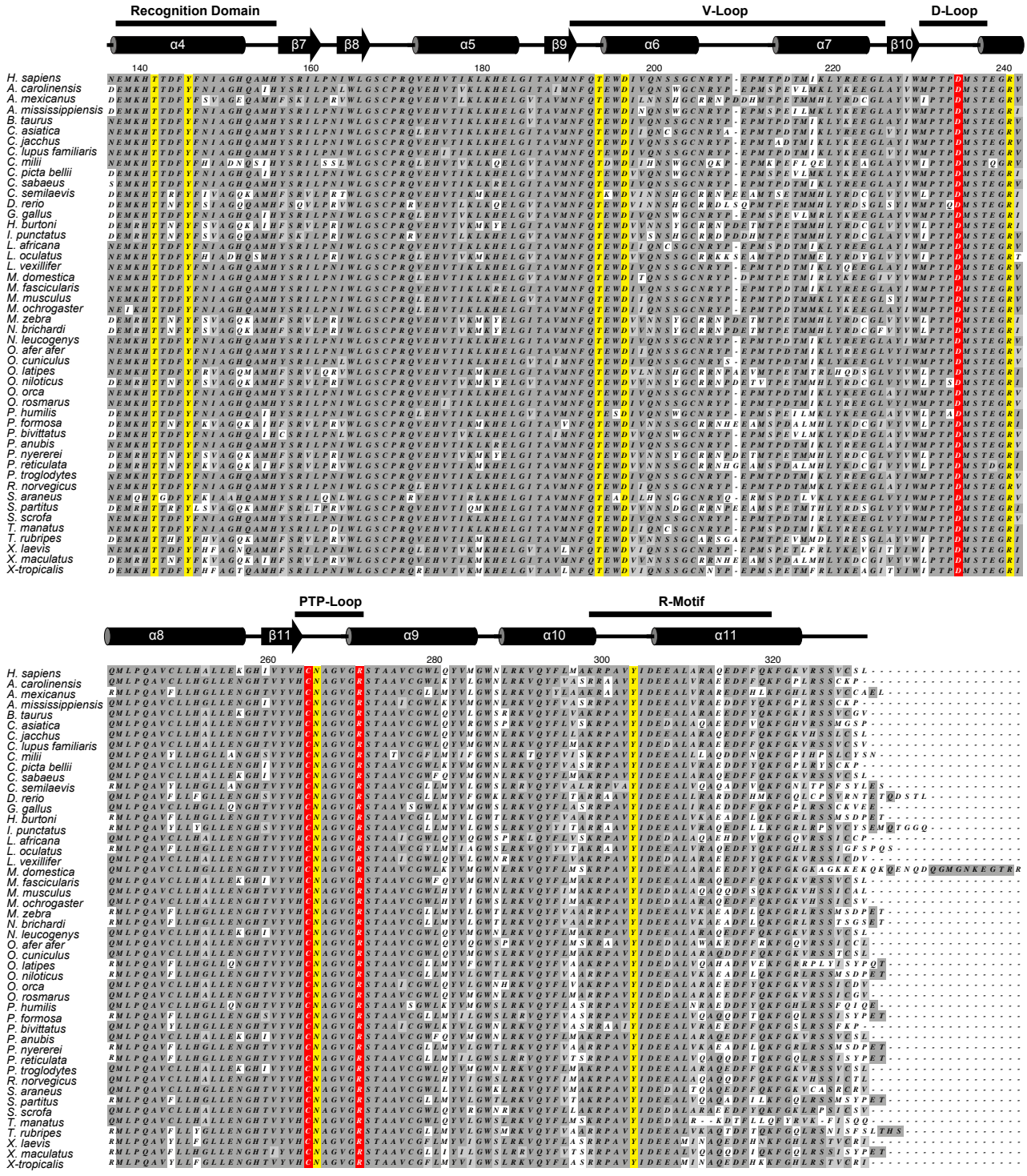
DSP
Recognition Domain
V-Loop
D-Loop
α4
β7
β8
α5
β9
α6
α7
β10
PTP-Loop
R-Motif
α8
β11
α9
α10
α11
H. sapiens
A. carolinensis
A. mexicanus
A. mississippiensis
B. taurus
C. asiatica
C. jacchus
C. lupus familiaris
C. milii
C. picta bellii
C. sabaeus
C. semilaevis
D. rerio
G. gallus
H. burtoni
I. punctatus
L. africana
L. oculatus
L. vexillifer
M. domestica
M. fascicularis
M. musculus
M. ochrogaster
M. zebra
N. brichardi
N. leucogenys
O. afer afer
O. cuniculus
O. latipes
O. niloticus
O. orca
O. rosmarus
P. humilis
P. formosa
P. bivittatus
P. anubis
P. nyererei
P. reticulata
P. troglodytes
R. norvegicus
S. araneus
S. partitus
S. scrofa
T. manatus
T. rubripes
X. laevis
X. maculatus
X-tropicalis

B

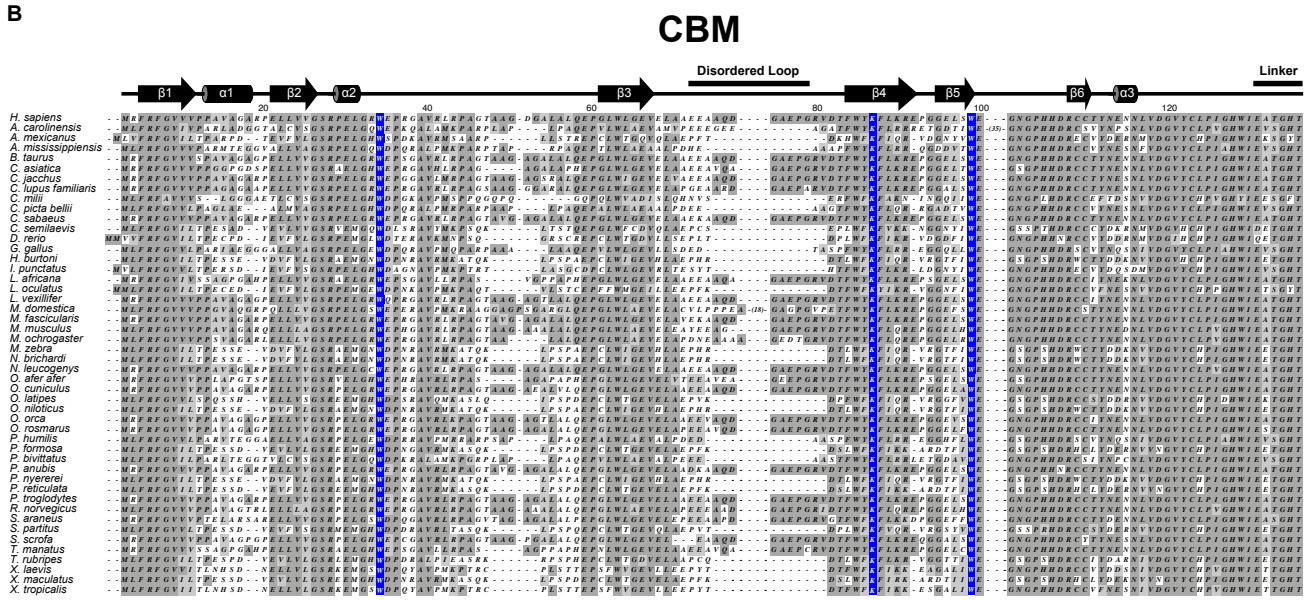
CBM
Disordered Loop
Linker
β1
α1
β2
α2
β3
β4
β5
β6
α3
H. sapiens
A. carolinensis
A. mexicanus
A. mississippiensis
B. taurus
C. asiatica
C. jacchus
C. lupus familiaris
C. milii
C. picta bellii
C. sabaeus
C. semilaevis
D. rerio
G. gallus
H. burtoni
I. punctatus
L. africana
L. oculatus
L. vexillifer
M. domestica
M. fascicularis
M. musculus
M. ochrogaster
M. zebra
N. brichardi
N. leucogenys
O. afer afer
O. cuniculus
O. latipes
O. niloticus
O. orca
O. rosmarus
P. humilis
P. formosa
P. bivittatus
P. anubis
P. nyererei
P. reticulata
P. troglodytes
R. norvegicus
S. araneus
S. partitus
S. scrofa
T. manatus
T. rubripes
X. laevis
X. maculatus
X. tropicalis

Figure S3

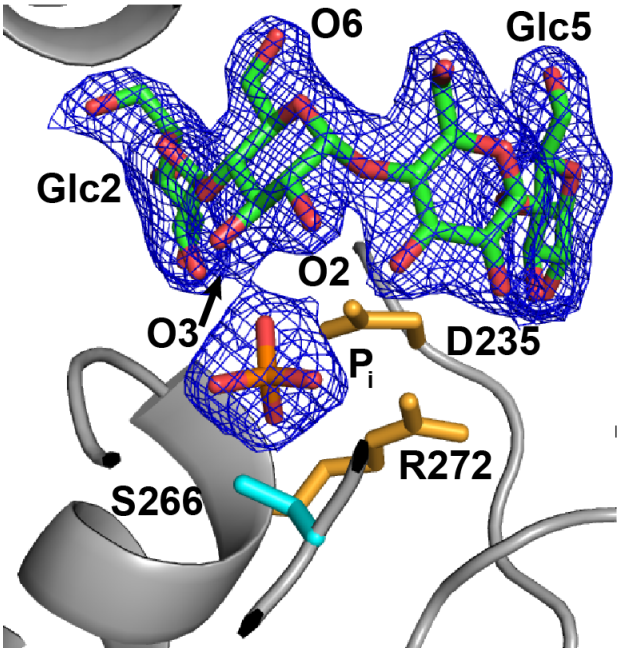
O6
Glc5
Glc2
O2
O3
D235
Pi
R272
S266

Figure S4

A

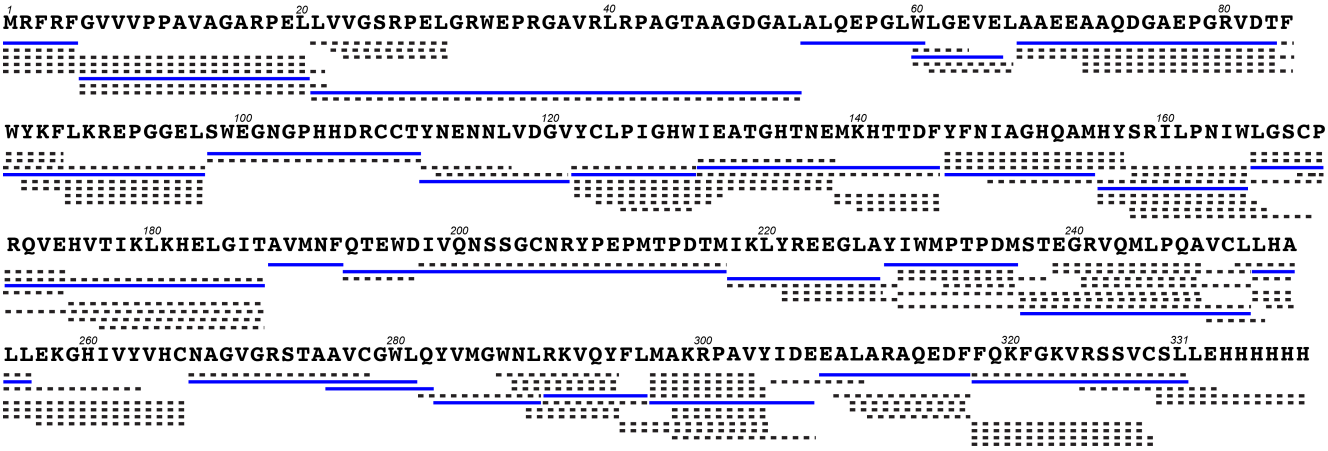
MRFRFGVVVPPAVAGARPELLVVGSRPELGRWEPRGAVRLRPAGTAAGDGALALQEPGLWLGEVELAAEEAAQDGAEPGRVDTF
WYKFLKREPGGELSWEGNGPHHDRCCTYNENNLVDGVYCLPIGHWIEATGHTNEMKHTTDFYFNIAGHQAMHYSRILPNIWLGSCP
RQVEHVTIKLKHELGITAVMNFQTEWDIVQNSSGCNRYPEPMTPDTMIKLYREEGLAYIWMPTPDMSTEGRVQMLPQAVCLLHA
LLEKGHIVYVHCNAGVGRSTAAVCGWLQYVMGWNLRKVQYFLMAKRPAVYIDEEALARAQEDFFQKFGKVRSSVCSLLEHHHHHH

B

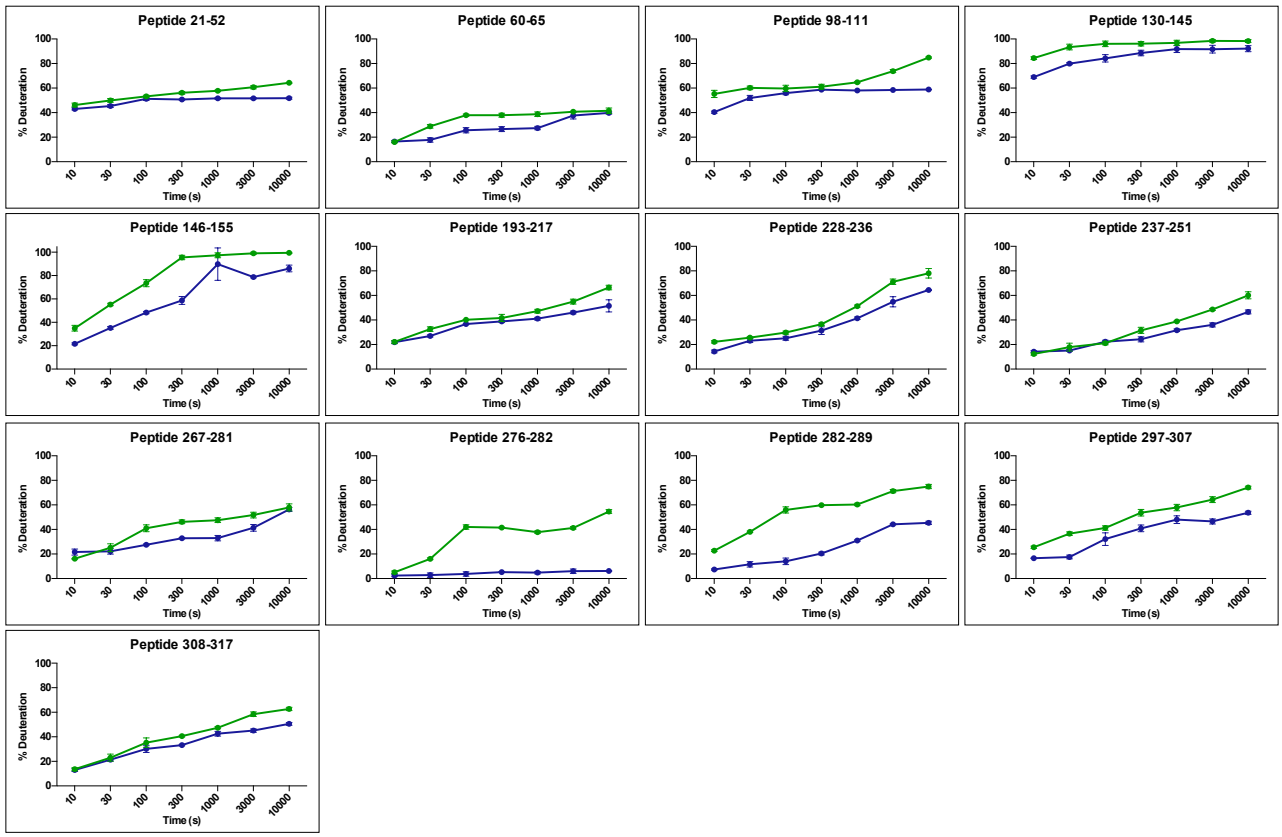
Peptide 21-52
Peptide 60-65
Peptide 98-111
Peptide 130-145
Peptide 146-155
Peptide 193-217
Peptide 228-236
Peptide 237-251
Peptide 267-281
Peptide 276-282
Peptide 282-289
Peptide 297-307
Peptide 308-317
% Deuteration
Time (s)

C

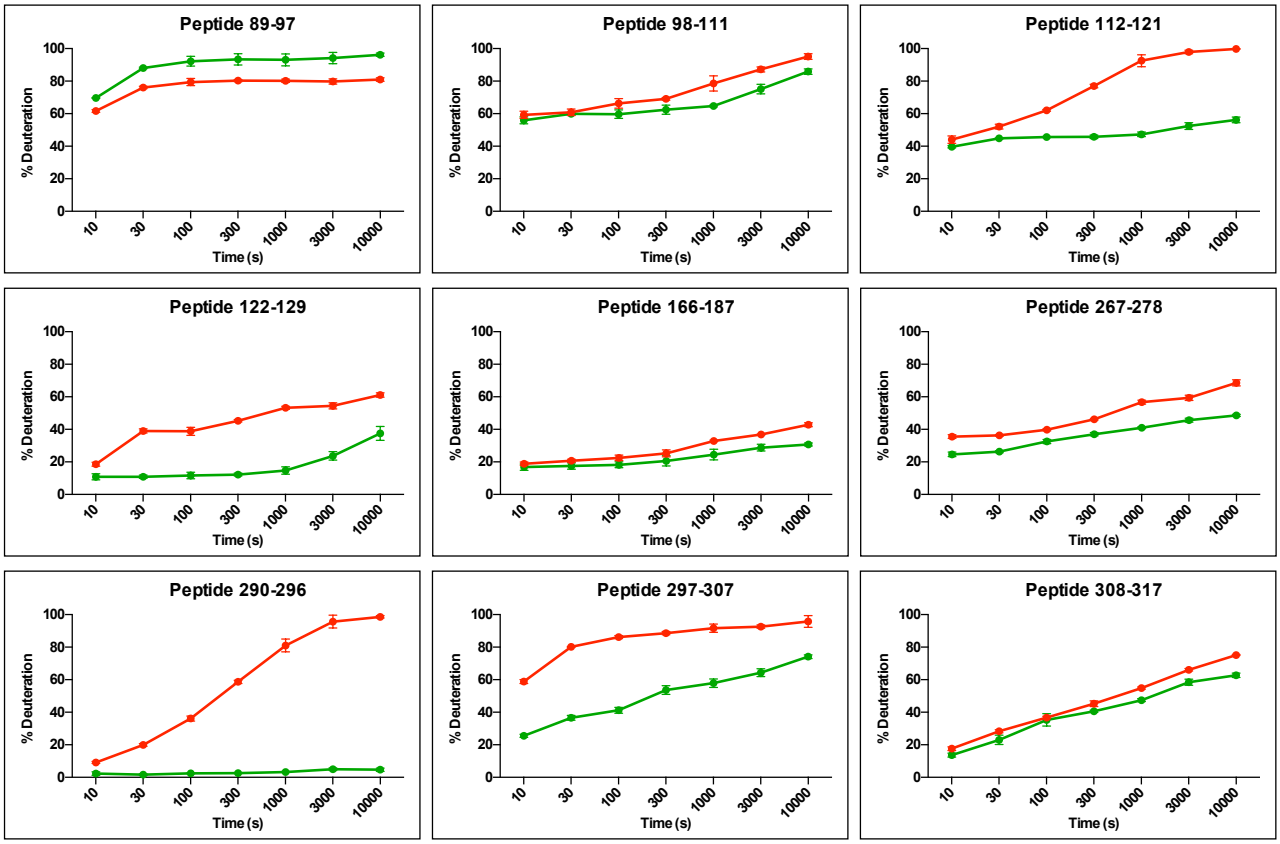
Peptide 89-97
Peptide 98-111
Peptide 112-121
Peptide 122-129
Peptide 166-187
Peptide 267-278
Peptide 290-296
Peptide 297-307
Peptide 308-317
% Deuteration
Time (s)
10
30
100
300
1000
3000
10000
0
20
40
60
80
100

Figure S5

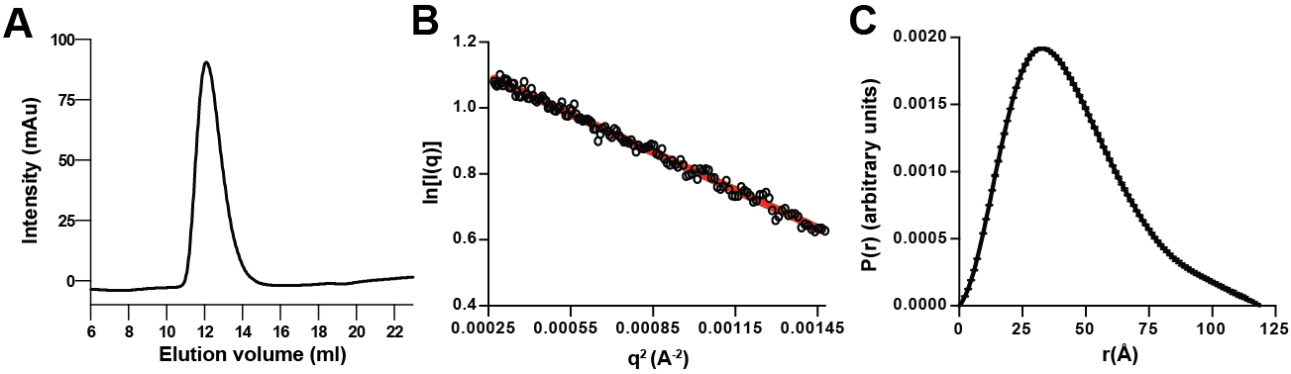
A
Intensity (mAu)
Elution volume (ml)
0
25
50
75
100
6
8
10
12
14
16
18
20
22
B
ln[I(q)]
q² (A⁻²)
0.4
0.6
0.8
1.0
1.2
0.00025
0.00055
0.00085
0.00115
0.00145
C
P(r) (arbitrary units)
r(Å)
0.0000
0.0005
0.0010
0.0015
0.0020
0
25
50
75
100
125

Figure S6

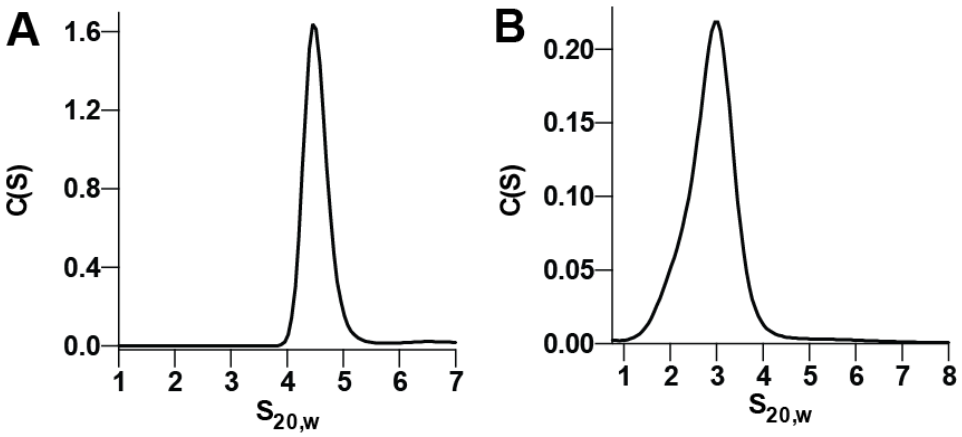

SUPPLEMENTAL FIGURE LEGENDS

Figure S1, related to Figure 2. Structure comparison of glucan phosphatases laforin, SEX4 and LSF2.

Ribbon diagrams of the glucan phosphatases laforin, Starch EXcess4 (SEX4), and Like Sex Four2 (LSF2) with a star indicating the DSP domain active site. The laforin dimer interface is spatially positioned similar to the SEX4 and LSF2 CT-motif.

Figure S2, related to Figure 2 and Figure 3. Alignments of laforin orthologs.

(A) Alignment of the DSP domain of laforin vertebrate orthologs. Secondary structure elements are depicted above the primary sequence and DSP motifs are labeled. The catalytic triad residues D235, C266, and R272 are highlighted in red and residues interacting with maltohexaose are in yellow.

(B) Alignment of the CBM domain of laforin vertebrate orthologs. Secondary structure elements are depicted above the primary sequence. Critical residues for glycogen binding are highlighted in blue.

Figure S3, related to Figure 2. The laforin catalytic triad.

Close-up of the laforin DSP domain active site, showing a ribbon diagram of maltohexaose (green) and phosphate (orange) with 2Fo-Fc electron density map (1.3 σ). Glucose moieties in the maltohexaose chain are numbered from non-reducing to reducing end. Side chains of the catalytic triad are displayed, D235 (yellow), S266 (C266 in WT laforin, teal), and R272 (yellow). The O2 and O3 hydroxyls of Gl3 are pointing towards the active site with the O6 hydroxyl in solvent.

Figure S4, related to Figure 4. Deuterium exchange mass spectrometry (DXMS) peptide maps and peptide graphs.

(A) Sequence coverage map of identified pepsin-digested laforin peptides. A total of 134 high-quality peptides were detected. Solid blue lines indicate the 27 peptides utilized in the analysis. Dashed lines indicate peptides that were not used but were examined. Laforin primary sequence is above the corresponding peptides.

(B) Line graphs depicting peptides that exhibited a > 10% change in deuterium incorporation in the presence versus absence of glycogen. Data shown as green represents percentages of deuterium incorporation in glycogen-free laforin and blue represents glycogen-bound laforin. Percent deuterium incorporation is shown in a time-dependent manner.

(C) Line graphs depicting peptides that exhibited a > 10% change in deuterium incorporation for laforin Y294N versus laforin WT. Data shown as red represents percentages of deuterium incorporation for Y294N and green represents WT. Percent deuterium incorporation is shown in a time-dependent manner.

Figure S5, related to Figure 6. Size exclusion chromatography-small angle x-ray scattering (SEC-SAXS) analysis of laforin.

(A) Size exclusion chromatography profile of laforin C266S loaded onto a Superdex 75 10/300 GL (GE Healthcare) reveals that laforin elutes as a single species.

(B) Guinier plot of the low *q* region of the x-ray scattering data allows measurement of R_g = 33.9 ± 0.2 Å for laforin.

(C) The distance distribution P(r) function of SAXS scattering data of laforin.

Figure S6, related to Figure 7. Analytical ultracentrifugation analysis of laforin.

(A) Laforin WT sedimentation coefficient distribution as determined by sedimentation velocity analytical ultracentrifugation.

(B) Laforin F321S sedimentation coefficient distribution as determined by sedimentation velocity analytical ultracentrifugation.

SUPPLEMENTAL TABLE 1, related to Figures 2, 3, 5, and 6.

Table S1: T_m of laforin and laforin mutants	
Protein	**T_m (°C)**
WT	49.74 ± 0.11
CS	50.28 ± 0.02
V8A	50.13 ± 0.28
W32G	44.56 ± 0.11
K87A	50.30 ± 0.40
W99A	50.35 ± 0.12
I126T	49.83 ± 0.10
T142A	49.03 ± 0.55
R171H	52.78 ± 0.08
D197A	51.50 ± 0.03
M236A	50.04 ± 0.13
G240S	49.53 ± 0.10
L251A	44.90 ± 0.15
Y294N	49.14 ± 0.35
P301L	35.70 ± 0.29
F321S	36.80 ± 0.03

SUPPLEMENTAL EXPERIMENTAL PROCEDURES

Cloning, Protein Expression, and Protein Purification

H. sapiens (Hs) laforin residues 1-328 was expressed from pET28b (Novagen) as an N-terminal His_6 tag fusion and Hs-laforin 1-331 was expressed from pET21a (Novegen), as previously described (Gentry et al., 2007; Sanchez-Martin et al., 2013). All point mutants were created using a site-directed mutagenesis kit (Agilent). DNA was sequenced (Beckman Coulter Genomics) and verified using MacVector. Wild-type and mutant proteins were expressed in BL21-CodonPlus *E. coli* cells grown at 37˚C in 2xYT media to OD_{600} = 0.5 to 0.7, placed on ice for 20 min, induced with 1mM isopropyl β-D-thigalactoside, cells were then grown at 20˚C for 14 h, and harvested by centrifugation. Cells were lysed in 20 mM Tris-HCl, pH 7.5, 100 mM NaCl,

and 2 mM DTT, centrifuged to remove debris, and soluble proteins were loaded onto an IMAC column (Bio-Rad) using a Profinia Purification system (Bio-Rad). The elution fraction was desalted and a second IMAC column purification was performed. Following affinity purification, a HiLoad 16/60 Superdex 200 size exclusion column (GE Healthcare) was used for final purification equilibrated with size exclusion buffer (20 mM Tris pH 7.5, 100 mM NaCl and 2 mM DTT). Chemicals were obtained from Sigma-Aldrich, unless otherwise stated.

Crystal Structure Determination

Single, high quality native laforin-C266S crystals were grown at 4˚C via hanging drop vapor diffusion using a Mosquito liquid handling robot (TTP Labtech). Crystals were grown by combining 5.2 mg/ml in size exclusion buffer with 250 mM maltohexaose, incubated overnight, and combined with 0.19 M Sodium Acetate, 0.1 M Sodium Citrate, 25.5% PEG4000, and 15% Glycerol, pH=5 in a 1:3 ratio. Tungstate derivatives were grown by combining 4.7 mg/ml laforin in size exclusion buffer with 250 mM maltohexaose, 0.17 M Sodium Acetate, 0.08 M Sodium Citrate, 25.5% PEG4000, 15% Glycerol, and 30 mM Sodium Tungstate, pH=5 in a 1:3 ratio. Crystals were snap frozen in liquid nitrogen and data collected on the 22-ID beamline of SER-CAT at the Advanced Photon Source, Argonne National Laboratory. Native crystals diffracted to 2.4 Å resolution while tungstate derivatives diffracted to 3.0 Å (**Table SI**). Data was processed using HKL2000 (Otwinowski and Minor, 1997). The structure was determined via tungstate SAD using Phenix (Adams et al., 2010), employing HYSS (Grosse-Kunstleve and Adams, 2003), PHASER (McCoy et al., 2007), and RESOLVE (Terwilliger et al., 2008) to locate seven tungstate sites, obtain phase information, perform density modification, and generate an initial structural model. The structure was then built and refined by iterative model building and refinement using Coot (Emsley et al., 2010) and Refmac5 (Murshudov, 1997). Residues 69-79 of both molecules were not observed in electron density and not modeled. Areaimol and sc within CCP4 were used for analysis (Winn et al., 2011). MolProbity was used for structural validation (Chen et al., 2010). Molecular graphics were prepared using Pymol (Schrodinger, 2010). Comparative structure analysis were performed using Dali (Holm and Rosenstrom, 2010). Amino acid conservation was analyzed using ConSurf (Landau et al., 2005).

Phosphatase Assays

We utilized an established phosphatase assay that employs malachite green to quantify inorganic phosphate release from glycogen (Sherwood et al., 2013; Tagliabracci et al., 2008; Tagliabracci et al., 2007). Reactions were performed at room temperature in 20 µL reactions,

containing 1x phosphatase buffer (100 mM sodium acetate, 50 mM bis-Tris, 50 mM Tris-HCl, pH 7.0), 2 mM DTT, 45 µg glycogen, and 100 ng protein. Assays were performed in the linear range with respect to time and glycogen concentration using parameters previously described (Tagliabracci et al., 2008; Tagliabracci et al., 2011; Tagliabracci et al., 2007). Laforin proteins were incubated with glycogen for 20 minutes. The reaction was stopped by the addition of 20 µL of 100 mM *N*-ethylmaleamide and 80 µL of malachite green reagent, which has been demonstrated to rapidly quench the reaction (Gentry et al., 2007; Sherwood et al., 2013; Worby et al., 2006). Absorbance was measured at 620 nm. The assay was performed with each protein six times or more to determine specific activity. Laforin and variants were found to not efficiently utilize traditional PTP small molecule substrates like para-nitrophenylphosphate (pNPP) and 3-O-methylfluorescein phosphate (OMFP), a common feature of atypical DSPs (Gottlin et al., 1996; Taylor et al., 2000).

Glycogen Binding Assays

Glycogen binding assays were performed as previously described with the following modifications (McBride et al., 2009). We performed the glycogen binding assay with WT laforin in triplicate with increasing amounts of glycogen from 0.09 mg/ml to 187.5 mg/ml. We found that 64 mg/ml glycogen was sufficient to bind 5 ug of WT laforin, and was utilized for all subsequent assays. Concanavalin A (ConA) Agarose beads (Sigma) were washed three times in binding buffer (67 mM Na-HEPES pH 7.5, 0.2 mM $CaCl_2$, 10 mM $MgCl_2$, 1 mM $MnCl_2$). 16 mg of rabbit liver glycogen was added to 250 µL ConA solution and incubated for 1 hr at 4˚C on a neutator. The mixture was then centrifuged at 9,000 x g for 30 s and washed three times with buffer. Protease Inhibitor Cocktail (100 mM 4-(2-Aminoethyl)benzenesulfonyl fluoride hydrochloride, 100 mM benzamidine hydrochloride, 0.1 mM leupeptin, 0.1 mM E64), 5 µg of His_6-tagged protein, and 1 mM DTT was added to 33 µl of the ConA-glycogen mixture. The mixture was incubated for 1 hr at 4˚C on a neutator, centrifuged at 9,000 x g for 30 s, and sample collected as the supernatant (S) fraction. The beads were washed five times with 750 µl of buffer followed by centrifugation at 9,000 x g for 30 s. Following the final wash, beads were resuspended in an equivalent volume of SDS-PAGE buffer and heated to 95˚ C to release any bound proteins. Samples from the supernatant and pellet were separated by SDS-PAGE and proteins were visualized by Western analysis using an α-HIS antibody (NeuroMab). The assay was performed with each protein five times or more. Similar results were obtained at room temperature and 4˚C.

Hydrogen Deuterium Exchange Mass Spectrometry (DXMS)

DXMS experiments, measuring the location and rate of deuterium uptake via the difference in peptide mass between pre- and post-incubation in D_2O buffer, were performed as previously described (Hamuro et al., 2004; Hsu et al., 2009; Pantazatos et al., 2004). For laforin, 134 high-quality peptides with 100% coverage of laforin was obtained with 10 μg of protein per sample with a ratio of 5.3 μl :10.6 μl : 4 μl of protein : buffer : exchange quench solution (5.3% v/v formic acid, 15% v/v glycerol, 0.8 M GuHCl, 39 mM TCEP, pH 2.4) while using a 30 mg/mL porcine pepsin-immobilized protease column (16 μl bed volume) (Sigma; immobilized on Poros 20 AL medium from PerSeptive Biosystems) with a flow rate of 20 μL/min. Eluted peptides were analyzed by an LCQ Classic (Thermo Finnigan Inc.) electrospray ion trap-type mass spectrometer. Mass spectroscopy data were acquired in MS1 profile mode and data-dependent MS1:MS2 mode. To achieve high-resolution analysis of deuterium incorporation, we defined 27 peptides as the smallest peptide sequences that are resolved by overlapping peptides and calculated the mass gain for each peptide at the time points defined.

Wild-type and mutant laforin were incubated for varying time either alone or with glycogen at 4˚C (rabbit liver Type III, Sigma-Aldrich; 5 mg/mL). Exchange of laforin with and without glycogen was performed three independent times, with all samples prepared in triplicate. Back exchange correction for each peptide was also determined (Zhang and Smith, 1993). SEQUEST (Thermo Finnigan, Inc.) was utilized to identify the sequences of parent peptide ions from the collected MS/MS data. DXMS Explorer (Sierra Analytics, Modesto, CA) (Hamuro et al., 2003) data reduction software was used to confirm peptide identifications for the correct comparison of undeuterated and deuterated peptides. All selected peptides first passed the quality control threshold established by the software and then were manually checked for the mass envelope fitting with the calculated mass envelope for data reduction. The highest signal/noise ion was picked if multiple ionization charges (1, 2, or 3) of a peptide were detected. Percent deuteration was calculated as the number of deuterium ions incorporated into a given peptide at a fixed time divided by the maximum level incorporated at equilibrium of FD samples. Ribbon maps were created from individual peptide graphs depicting regional levels of deuterium incorporation and represent the average percent change in deuteration with a standard deviation of <2% between experiments.

Differential Scanning Fluorimetry (DSF)

Maltose through maltoheptaose were obtained from Carbosynth and Sigma. DP11, DP17 and DP24 were obtained from Elicityl. Maltoligosaccharides were dissolved in DSF buffer (50 mM

HEPES pH 7.5, 100 mM NaCl, 2 mM DTT) and combined with 5X SYPRO Orange Protein Gel Stain and 2 µM of protein at a final volume of 40 µl in DSF buffer. Laforin melting was monitored on a CFX96 Real-Time PCR system (BioRad) from 20 to 90 ˚C at a rate of 1 ˚C/50 s. The T_m was determined by fitting the first derivatives of the data with a Gaussian distribution using Prism. Each protein was analyzed in triplicate. Data was analyzed using Prism one site specific binding with Hill slope, Y=Bmax*[oligosaccharide]^h/(Kd^h + [oligosaccharide]^h, or two site specific binding, Y=Bmax*[oligosaccharide/K_d+oligosaccharide]. The range of oligosaccharides used were 0-12.5 mM for DP11, DP17, and DP24, and 0-12.5 mM for maltoheptaose.

Small Angle X-ray Scattering (SAXS)

Size-Exclusion Chromatography – Small Angle X-ray Scattering (SEC-SAXS) experiments were performed at BioCAT, (beamline 18-ID, Advanced Photon Source at Argonne National Labs) (Mathew et al., 2004). The camera included a focused 12KeV (1.03 Å) x-ray beam, a 1.5mm quartz capillary sample cell, a sample to detector distance of ~2.5m, and a Mar165 CCD detector (Rayonix). The q-range sampled was 0.0065 – 0.3 $Å^{-1}$. An inline AKTA Pure (GE Life Sciences) was used to load 200 µL of a 4.7 mg/mL laforin solution onto a Superdex 75 10/300 column in gel filtration buffer without glycerol (GE Life Sciences) at room temperature. A series of 1 s exposures, spaced 5s apart, were collected across the elution peak and analyzed (Petoukhov et al., 2007). Exposures before the elution of the sample were averaged and used as the buffer curve. Data for the protein (co-incident with the UV peak on the chromatogram) were corrected for background scattering by subtracting the buffer curve. Guinier analysis demonstrated that the system is monodisperse with particles that have a Rg = 33.9 ± 0.2 Å. (**Figure S5A**). Theoretical scattering curves were calculated using FoXS (Schneidman-Duhovny et al., 2010). Pair-distance distribution function (P(r)) demonstrated a well-defined Dmax = 119 Å (**Figure S5B**) (Svergun, 1992). From this the real space Rg was also calculated (35.0 Å) and found to be in good agreement with that determined by Guinier analysis, thus providing an independent indicator of data quality. *ab initio* reconstruction of the average molecular envelope was accomplished by generating fifty DAMMIF runs followed by alignment and averaging using DAMAVER (Volkov and Svergun, 2003). The average molecular envelope was superimposed with the crystal structure using supcomb (Kozin and Svergun, 2001).

Analytical Ultracentrifugation (AU)

Sedimentation velocity experiments were conducted using a Beckman XL-I analytical ultracentrifuge (Beckman-Coulter, Fullerton, CA). Protein was concentrated to 5 µM in size

exclusion buffer. Sample was analyzed at 40,000 and 4 °C and absorption measurements taken at 280 nm. Measurements of sedimentation coefficient distributions between 0.1 and 8 s were analyzed using numerical solutions of the Lamm equation implemented in Sedfit (Schuck et al., 2002). SEDNTERP (Laue et al., 1992) was used to calculate buffer density, viscosity, and partial specific volumes of the proteins. Standard conditions of 20 ˚C and water (s20,w) were calculated from experimentally determined s-values.

SUPPLEMENTAL REFERENCES

Adams, P.D., Afonine, P.V., Bunkoczi, G., Chen, V.B., Davis, I.W., Echols, N., Headd, J.J., Hung, L.W., Kapral, G.J., Grosse-Kunstleve, R.W.*, et al.* (2010). PHENIX: a comprehensive Python-based system for macromolecular structure solution. Acta Crystallogr D Biol Crystallogr *66*, 213-221.

Chen, V.B., Arendall, W.B., 3rd, Headd, J.J., Keedy, D.A., Immormino, R.M., Kapral, G.J., Murray, L.W., Richardson, J.S., and Richardson, D.C. (2010). MolProbity: all-atom structure validation for macromolecular crystallography. Acta Crystallogr D Biol Crystallogr *66*, 12-21.

Emsley, P., Lohkamp, B., Scott, W.G., and Cowtan, K. (2010). Features and development of Coot. Acta Crystallogr D Biol Crystallogr *66*, 486-501.

Gentry, M.S., Dowen, R.H., 3rd, Worby, C.A., Mattoo, S., Ecker, J.R., and Dixon, J.E. (2007). The phosphatase laforin crosses evolutionary boundaries and links carbohydrate metabolism to neuronal disease. J Cell Biol *178*, 477-488.

Gottlin, E.B., Xu, X., Epstein, D.M., Burke, S.P., Eckstein, J.W., Ballou, D.P., and Dixon, J.E. (1996). Kinetic analysis of the catalytic domain of human cdc25B. J Biol Chem *271*, 27445-27449.

Grosse-Kunstleve, R.W., and Adams, P.D. (2003). Substructure search procedures for macromolecular structures. Acta Crystallogr D Biol Crystallogr *59*, 1966-1973.

Hamuro, Y., Anand, G.S., Kim, J.S., Juliano, C., Stranz, D.D., Taylor, S.S., and Woods, V.L., Jr. (2004). Mapping intersubunit interactions of the regulatory subunit (Rlalpha) in the type I holoenzyme of protein kinase A by amide hydrogen/deuterium exchange mass spectrometry (DXMS). J Mol Biol *340*, 1185-1196.

Hamuro, Y., Coales, S.J., Southern, M.R., Nemeth-Cawley, J.F., Stranz, D.D., and Griffin, P.R. (2003). Rapid analysis of protein structure and dynamics by hydrogen/deuterium exchange mass spectrometry. J Biomol Tech *14*, 171-182.

Holm, L., and Rosenstrom, P. (2010). Dali server: conservation mapping in 3D. Nucleic Acids Res *38*, W545-549.

Hsu, S., Kim, Y., Li, S., Durrant, E.S., Pace, R.M., Woods, V.L., Jr., and Gentry, M.S. (2009). Structural insights into glucan phosphatase dynamics using amide hydrogen-deuterium exchange mass spectrometry. Biochemistry *48*, 9891-9902.

Kozin, M.B., and Svergun, D.I. (2001). Automated matching of high- and low-resolution structural models. Journal of Applied Crystallography *34*, 33-41.

Landau, M., Mayrose, I., Rosenberg, Y., Glaser, F., Martz, E., Pupko, T., and Ben-Tal, N. (2005). ConSurf 2005: the projection of evolutionary conservation scores of residues on protein structures. Nucleic Acids Res *33*, W299-302.

Mathew, E., Mirza, A., and Menhart, N. (2004). Liquid-chromatography-coupled SAXS for accurate sizing of aggregating proteins. Journal of synchrotron radiation *11*, 314-318.

McBride, A., Ghilagaber, S., Nikolaev, A., and Hardie, D.G. (2009). The glycogen-binding domain on the AMPK beta subunit allows the kinase to act as a glycogen sensor. Cell Metab *9*, 23-34.

McCoy, A.J., Grosse-Kunstleve, R.W., Adams, P.D., Winn, M.D., Storoni, L.C., and Read, R.J. (2007). Phaser crystallographic software. J Appl Crystallogr *40*, 658-674.

Murshudov, G.N. (1997). Refinement of macromolecular structures by the maximum-likelihood method. Acta Crystallogr D Biol Crystallogr *53*, 240-255.

Otwinowski, Z., and Minor, W. (1997). Processing of X-ray diffraction data collected in oscillation mode. Method Enzymol *276*, 307-326.

Pantazatos, D., Kim, J.S., Klock, H.E., Stevens, R.C., Wilson, I.A., Lesley, S.A., and Woods, V.L., Jr. (2004). Rapid refinement of crystallographic protein construct definition employing enhanced hydrogen/deuterium exchange MS. Proc Natl Acad Sci U S A *101*, 751-756.

Petoukhov, M.V., Konarev, P.V., Kikhney, A.G., and Svergun, D.I. (2007). ATSAS 2.1 - towards automated and web-supported small-angle scattering data analysis. Journal of Applied Crystallography *40*, S223-S228.

Sanchez-Martin, P., Raththagala, M., Bridges, T.M., Husodo, S., Gentry, M.S., Sanz, P., and Roma-Mateo, C. (2013). Dimerization of the glucan phosphatase laforin requires the participation of cysteine 329. PLoS One *8*, e69523.

Schneidman-Duhovny, D., Hammel, M., and Sali, A. (2010). FoXS: a web server for rapid computation and fitting of SAXS profiles. Nucleic Acids Research *38*, W540-W544.

Schrodinger, L. (2010). The PyMOL MOlecular Graphics System, Version 1.3.

Sherwood, A.R., Paasch, B.C., Worby, C.A., and Gentry, M.S. (2013). A malachite green-based assay to assess glucan phosphatase activity. Anal Biochem *435*, 54-56.

Svergun, D.I. (1992). Determination of the Regularization Parameter in Indirect-Transform Methods Using Perceptual Criteria. Journal of Applied Crystallography *25*, 495-503.

Tagliabracci, V.S., Girard, J.M., Segvich, D., Meyer, C., Turnbull, J., Zhao, X., Minassian, B.A., Depaoli-Roach, A.A., and Roach, P.J. (2008). Abnormal metabolism of glycogen phosphate as a cause for lafora disease. J Biol Chem *283*, 33816-33825.

Tagliabracci, V.S., Heiss, C., Karthik, C., Contreras, C.J., Glushka, J., Ishihara, M., Azadi, P., Hurley, T.D., DePaoli-Roach, A.A., and Roach, P.J. (2011). Phosphate incorporation during glycogen synthesis and Lafora disease. Cell Metab *13*, 274-282.

Tagliabracci, V.S., Turnbull, J., Wang, W., Girard, J.M., Zhao, X., Skurat, A.V., Delgado-Escueta, A.V., Minassian, B.A., Depaoli-Roach, A.A., and Roach, P.J. (2007). Laforin is a glycogen phosphatase, deficiency of which leads to elevated phosphorylation of glycogen in vivo. Proc Natl Acad Sci U S A *104*, 19262-19266.

Taylor, G.S., Maehama, T., and Dixon, J.E. (2000). Inaugural article: myotubularin, a protein tyrosine phosphatase mutated in myotubular myopathy, dephosphorylates the lipid second messenger, phosphatidylinositol 3-phosphate. Proc Natl Acad Sci U S A *97*, 8910-8915.

Terwilliger, T.C., Grosse-Kunstleve, R.W., Afonine, P.V., Moriarty, N.W., Zwart, P.H., Hung, L.W., Read, R.J., and Adams, P.D. (2008). Iterative model building, structure refinement and density modification with the PHENIX AutoBuild wizard. Acta Crystallogr D Biol Crystallogr *64*, 61-69.

Volkov, V.V., and Svergun, D.I. (2003). Uniqueness of ab initio shape determination in small-angle scattering. Journal of Applied Crystallography *36*, 860-864.

Winn, M.D., Ballard, C.C., Cowtan, K.D., Dodson, E.J., Emsley, P., Evans, P.R., Keegan, R.M., Krissinel, E.B., Leslie, A.G., McCoy, A.*, et al.* (2011). Overview of the CCP4 suite and current developments. Acta Crystallogr D Biol Crystallogr *67*, 235-242.

Worby, C.A., Gentry, M.S., and Dixon, J.E. (2006). Laforin: A dual specificity phosphatase that dephosphorylates complex carbohydrates. J Biol Chem *281*, 30412-30418.

Zhang, Z., and Smith, D.L. (1993). Determination of amide hydrogen exchange by mass spectrometry: a new tool for protein structure elucidation. Protein science : a publication of the Protein Society *2*, 522-531.